



## Room-temperature ferroelectricity of SrTiO<sub>3</sub> films modulated by cation concentration

Fang Yang,<sup>1</sup> Qinghua Zhang,<sup>1</sup> Zhenzhong Yang,<sup>1</sup> Junxing Gu,<sup>1</sup> Yan Liang,<sup>1</sup> Wentao Li,<sup>1</sup> Weihua Wang,<sup>1</sup> Kuijuan Jin,<sup>1,2</sup> Lin Gu,<sup>1,2</sup> and Jiandong Guo<sup>1,2,a)</sup>

<sup>1</sup>Beijing National Laboratory for Condensed-Matter Physics and Institute of Physics, Chinese Academy of Sciences, Beijing 100190, China

<sup>2</sup>Collaborative Innovation Center of Quantum Matter, Beijing 100871, China

(Received 25 June 2015; accepted 10 August 2015; published online 27 August 2015)

The room-temperature ferroelectricity of SrTiO<sub>3</sub> is promising for oxide electronic devices controlled by multiple fields. An effective way to control the ferroelectricity is highly demanded. Here, we show that the off-centered antisite-like defects in SrTiO<sub>3</sub> films epitaxially grown on Si (001) play the determinative role in the emergence of room-temperature ferroelectricity. The density of these defects changes with the film cation concentration sensitively, resulting in a varied coercive field of the ferroelectric behavior. Consequently, the room-temperature ferroelectricity of SrTiO<sub>3</sub> films can be effectively modulated by tuning the temperature of metal sources during the molecular beam epitaxy growth. Such an easy and reliable modulation of the ferroelectricity enables the flexible engineering of multifunctional oxide electronic devices. © 2015 AIP Publishing LLC.

[<http://dx.doi.org/10.1063/1.4929610>]

Ferroelectricity in complex oxides attracts extensive interests owing to the potential applications of ferroelectric thin films in nonvolatile random access memories and high-density data storage devices.<sup>1</sup> Strontium titanate (SrTiO<sub>3</sub>) has been widely used as substrates for oxide film growth.<sup>2–4</sup> More importantly, it is a so-called incipient ferroelectric, i.e., the central inversion symmetry in the unit cell can be readily broken by external perturbations, leading to the formation of electrical dipole and therefore the ferroelectricity in the material.<sup>5</sup> It would be exciting to integrate the ferroelectric SrTiO<sub>3</sub> substrates with films of other functionalized oxides for the next-generation all-oxide electronic devices controlled by multiple fields. To realize the applications, it is essential to tune the ferroelectricity, i.e., the polarization state or the coercive field. For example, high polarization and low coercive field are required in nonvolatile devices such as ferroelectric random access memories and ferroelectric field effect transistors.<sup>1</sup> The polarization states of ferroelectric materials can control the conducting behavior of the two dimensional electron gas at the interface of LaAlO<sub>3</sub>/SrTiO<sub>3</sub> effectively.<sup>4</sup> However, the reliable modulation of ferroelectricity in SrTiO<sub>3</sub> has not been experimentally achieved yet, not even the microscopic mechanism that plays the dominant role in the emergence of ferroelectricity in the material is being clarified.

Early studies reported ferroelectricity in SrTiO<sub>3</sub> at low temperatures can be induced by calcium doping,<sup>6</sup> electric field,<sup>7</sup> or isotope substitution.<sup>8</sup> SrTiO<sub>3</sub> film with tetragonal structure grown under low oxygen pressure can exhibit room-temperature ferroelectricity (RTFE);<sup>9</sup> however, this way tends to bring about oxygen vacancies which would deteriorate ferroelectricity in SrTiO<sub>3</sub>. Schlom *et al.* reported RTFE in strained epitaxial SrTiO<sub>3</sub> films,<sup>10,11</sup> but this method is limited by the film thickness and the choice of substrates.

RTFE was also reported in strain-free SrTiO<sub>3</sub> films, where Sr deficiency was believed to play an important role by different groups.<sup>12–14</sup> But the exact microscopic mechanism how RTFE can be induced by Sr deficiency is still under debate. Noh *et al.* proposed that RTFE is owing to the Sr-O-O vacancy clusters.<sup>13</sup> By density functional theory (DFT) calculations, Choi *et al.* have proposed that an off-centered antisite-like defect (OAD) in SrTiO<sub>3</sub>, composed of a Sr vacancy (V<sub>Sr</sub>) and an interstitial Ti atom (I<sub>Ti</sub>), can induce the ferroelectricity in SrTiO<sub>3</sub> at room temperature.<sup>15</sup> In this paper, we observed RTFE in epitaxial SrTiO<sub>3</sub> films grown on Si (001) substrates by piezo-response force microscopy (PFM). As revealed by scanning transmission electron microscope (STEM), the RTFE is originated from OADs at the atomic scale, while other possible factors can be neglected. Most importantly, the density of OADs changes sensitively with the cation concentration in the film, resulting in varied coercive field that can be tuned by the growth conditions.

SrTiO<sub>3</sub> (001) films were grown on *p*-type Si (001) substrates by oxide molecular beam epitaxy (MBE) method. Sr and Ti were evaporated in a molecular oxygen ambient using Knudsen effusion cells. The Sr and Ti flux rates were calibrated by monitoring the surface reconstructions during homoepitaxy of SrTiO<sub>3</sub> (110) with reflective high energy electron diffractions (RHEEDs).<sup>16</sup> The samples were resistively heated by passing through a direct current in the ultra-high vacuum chamber. The Si (001)-(2 × 1) surface was obtained by “flashing” recipe.<sup>17</sup> Then a half monolayer of Sr was deposited at a substrate temperature of 500 °C. The initial two monolayers of SrTiO<sub>3</sub> were prepared according to Ref. 11 as the buffer layer. SrTiO<sub>3</sub> films were grown by coevaporation method under 1.5 × 10<sup>-8</sup> mbar oxygen pressure with the substrate temperature at 430 °C. The Ti source temperature was unchanged at 1460 °C during deposition, while keeping the Sr source temperature at 417.4 °C gives the same evaporation rate. Different cation concentrations

<sup>a)</sup>Electronic mail: jdguo@iphy.ac.cn

were obtained by finely adjusting the Sr source temperature. In this work, we compared three typical samples, H-Sr/Ti, M-Sr/Ti, and L-Sr/Ti, grown at Sr source temperatures of 422°C, 415.4°C, and 413.4°C, with the ratio of Sr-to-Ti growth rate of 1.23, 0.91, and 0.82, respectively. A schematic picture shown in Fig. 1(a) depicts the structure and the epitaxial relationship between the film and the substrate. All the SrTiO<sub>3</sub> films have the same thickness of 30 monolayers (ML), i.e., 11.7 nm. The samples were post-annealed at 400°C under  $5 \times 10^{-6}$  mbar oxygen pressure for 1 h to reduce oxygen vacancies.

Domain writing and reading by PFM are commonly used to characterize the ferroelectric properties in thin films.<sup>12,18,19</sup> The signature of the ferroelectricity is the reversible polarization measured as the 180° contrast in PFM phase images.<sup>20</sup> We carried out a box-in-box switching measurement by a conductive PFM tip with alternative +10 and -10 V biases at room temperature. First, a  $5 \times 5 \mu\text{m}^2$  area was scanned with applying a DC bias voltage of +10 V by a Pt-coated conductive tip. Then the central  $2.5 \times 2.5 \mu\text{m}^2$  region was scanned with a reversed DC bias of -10 V, followed by the PFM imaging through the entire area to evaluate the piezoelectric response of the pre-written ferroelectric domain structure. The local piezo-response phase hysteresis loops were obtained by Dual AC Resonance Tracking (DART) mode to characterize the ferroelectricity and to further determine the coercive voltage (field).

The out-of-plane PFM phase image of the sample L-Sr/Ti shows the typical piezoelectric response, as displayed in Fig. 1(b). The positively and negatively polarized regions show a sharp contrast with the averaged phase difference of 180° (Fig. 1(d)), indicating that the writing/reading as well as reversal of polarization direction can be achieved on L-Sr/Ti. Therefore, the RTFE in the L-Sr/Ti film is evidenced.<sup>20</sup> The M-Sr/Ti film shows the similar RTFE characteristic,

while, in contrast, the same PFM measurement on the sample H-Sr/Ti shows a rather weak contrast between regions with opposite polarization directions (Fig. 1(c)). The phase difference between the two regions is vague and far from 180°. Besides, no hysteresis loop of the phase-voltage curve can be obtained in H-Sr/Ti, both indicating that the H-Sr/Ti is not ferroelectric.

The strain in the heteroepitaxial SrTiO<sub>3</sub> film as the origin of the observed ferroelectricity in L-Sr/Ti can be excluded, since the thickness (30 ML) is far beyond the range that the film can be affected by strain.<sup>11</sup> Moreover, it can also be ruled out that the RTFE arises from the tetragonal structure due to low oxygen pressure during growth because both L-Sr/Ti and H-Sr/Ti films are grown under the same oxygen pressure.<sup>9</sup> To investigate the microscopic mechanism of the RTFE in L-Sr/Ti in detail, we performed atomic-resolved cross sectional STEM measurements on both samples along the [100] direction. The high-angle annular dark field (HAADF) image of the H-Sr/Ti shows the homogenous and ideal cubic lattice structure. But, as shown in Figs. 2(a) and 2(b), excessive Ti atoms are clearly visible in the STEM images of L-Sr/Ti. Most of them occupy the interstitial positions displaced from the Sr site by about 1.6 Å along the six equivalent  $\langle 001 \rangle$  directions (Fig. 2(a)), while occasionally they are observed with a displacement from the Sr site by about 1.3 Å along the 12 equivalent  $\langle 110 \rangle$  directions.

The DFT calculations have revealed the stability of the defects associated by interstitial Ti atoms, i.e., the OADs composed of pairs of a  $V_{\text{Sr}}$  and an off-centered antisite-like  $I_{\text{Ti}}$  with displacement along  $\langle 001 \rangle$  (referred to as the  $\langle 001 \rangle$ -type hereafter) or along  $\langle 110 \rangle$  ( $\langle 110 \rangle$ -type), as illustrated in Figs. 2(e) and 2(f).<sup>15</sup> Using these structural models, and taking the  $V_{\text{Sr}}$  concentration as 18% that is determined by the evaporation rate ratio of Sr and Ti during MBE growth, also

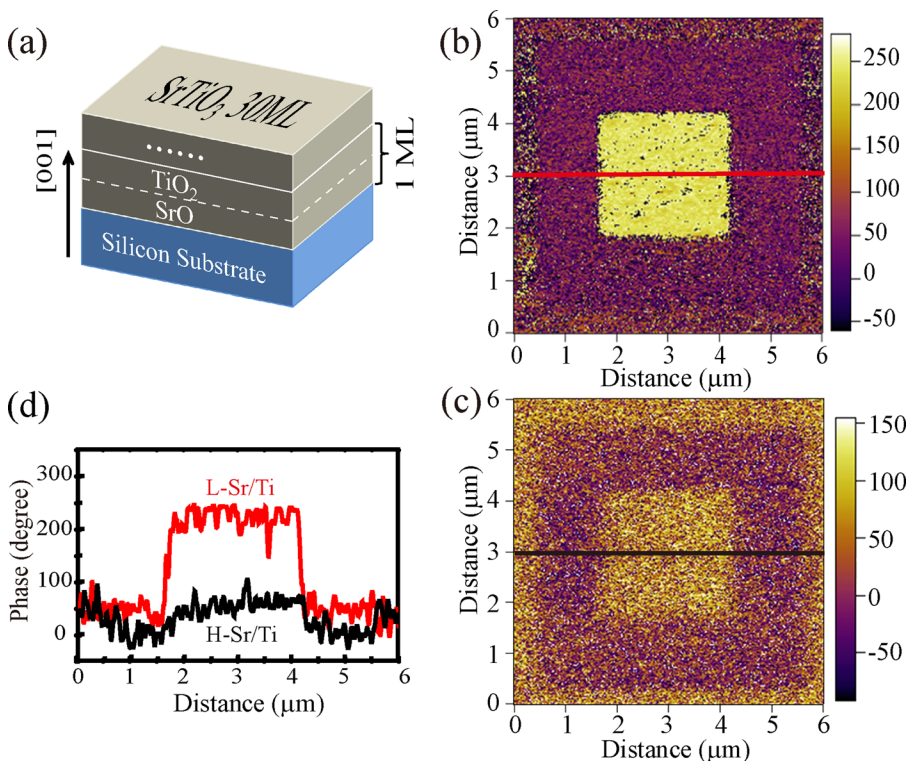


FIG. 1. (a) The schematic picture of SrTiO<sub>3</sub>/Si (001). Along the [001] direction, 1 ML of SrTiO<sub>3</sub> is composed of SrO and TiO<sub>2</sub> atomic layers with the height of 3.905 Å. The total thickness of the SrTiO<sub>3</sub> films is 11.7 nm. (b) and (c) PFM phase images after a box-in-box switching on the samples of L-Sr/Ti and H-Sr/Ti, respectively. A  $5 \times 5 \mu\text{m}^2$  box was polarized with the tip bias of +10 V, and then a smaller box,  $2.5 \times 2.5 \mu\text{m}^2$ , was subsequently scanned with the tip bias of -10 V. The color bars indicate the phase. (d) The line profiles of the lines in (b) (red) and (c) (black), respectively.

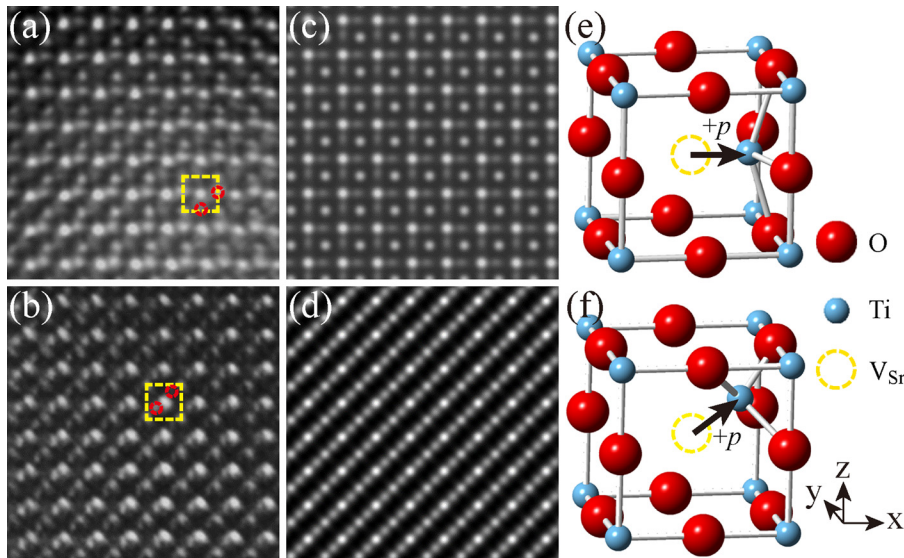


FIG. 2. (a) and (b) HAADF images of the SrTiO<sub>3</sub> films with the OADs of  $\langle 100 \rangle$ - and  $\langle 110 \rangle$ -types, respectively. The Sr atoms appear as bright dots, while Ti atoms appear as dim dots in the images. The unit cells are labeled by the dashed squares, and the interstitial Ti atoms are highlighted by the dashed circles, respectively. (c) and (d) The corresponding simulated STEM images with the Sr vacancy concentration of 18%. (e) and (f) The atomic configurations of OADs of  $\langle 100 \rangle$ - and  $\langle 110 \rangle$ -types, respectively. The electric dipoles along  $[100]$  and  $[110]$  directions are also indicated by the arrows.

consistent with the RBS characterizations,<sup>21</sup> we simulate the STEM images with satisfactory consistency, as presented in Figs. 2(c) and 2(d). It should be noted that, due to the large Coulomb repulsion between adjacent interstitial Ti atoms, there would not be multiple  $I_{Ti}$  in one unit cell, even in different types. The appearance of multiple  $I_{Ti}$  in one square [see Figs. 2(a) and 2(b)] is resulted from the overlap of multiple unit cells with different OADs along the cross sectional STEM imaging direction. This is also reproduced by the image simulation for the sample with a finite thickness (60 nm), as shown in Figs. 2(c) and 2(d). It is evident that the observed deviation of the STEM images from that of perfect SrTiO<sub>3</sub> is originated from the existence of OADs.

In the unit cell with an OAD, the separated  $V_{Sr}$  (negatively charged) and  $I_{Ti}$  (positively charged) lead the charge center being offset from the geometry center of the lattice, resulting in an electric dipole moment along the direction from  $V_{Sr}$  to  $I_{Ti}$ . The OADs with an identical displacement direction, i.e., the aligned dipoles will induce a certain electric polarization. Therefore, the OADs are responsible for the emergence of RTFE in the SrTiO<sub>3</sub> films.

Since the existence of OADs leads to the nonstoichiometry in the SrTiO<sub>3</sub> film, we try to control their density by adjusting the evaporation rates of metals in the MBE growth. As monitored by RHEED, high-quality layer-by-layer growth and the single crystallinity of the film can be obtained within a certain range of the Sr-to-Ti evaporation ratio from  $\sim 0.7$  to  $\sim 1.2$ .<sup>21</sup> The statistics over several HAADF images of L-Sr/Ti, M-Sr/Ti, and H-Sr/Ti with atomic resolution show the close dependence of OADs density on the averaged cation concentration in the film. It should be noted that, unlike the  $\langle 110 \rangle$ -type OADs, all of which can be observed in the cross sectional STEM images along  $[100]$ , the  $\langle 100 \rangle$ -type OADs with displacements along  $[010]$  and  $[0\bar{1}0]$  out of the six equivalent  $\langle 001 \rangle$  directions are invisible since the interstitial Ti atoms are right behind the Sr sites. We correct the statistics by assuming the  $\langle 001 \rangle$ -type OADs have no preferred displacement directions. As plotted in Fig. 3(a), the OADs concentration is 19% in L-Sr/Ti (Sr-to-Ti evaporation ratio of 0.82 during growth), while it is 9.3% in M-Sr/Ti (Sr-to-Ti ratio of 0.91 during growth). No OAD is observed in H-Sr/Ti (Sr-to-Ti ratio of

1.23 during growth). The OADs concentration can be tuned reliably by adjusting the MBE growth conditions.

Local piezo-response phase hysteresis loops of the samples were measured at room temperature. No hysteresis is obtained for H-Sr/Ti, while both L-Sr/Ti and M-Sr/Ti exhibit switchable square shapes with a phase difference of  $180^\circ$ , as shown in Fig. 3(b). The coercive voltage of the L-Sr/Ti and M-Sr/Ti is dramatically different as 5.7 V and 2.6 V, respectively. This can be easily understood that the absence of OADs in H-Sr/Ti results in the zero net polarization; and the higher concentration of OADs in L-Sr/Ti results in larger polarization than in M-Sr/Ti with a lower OADs

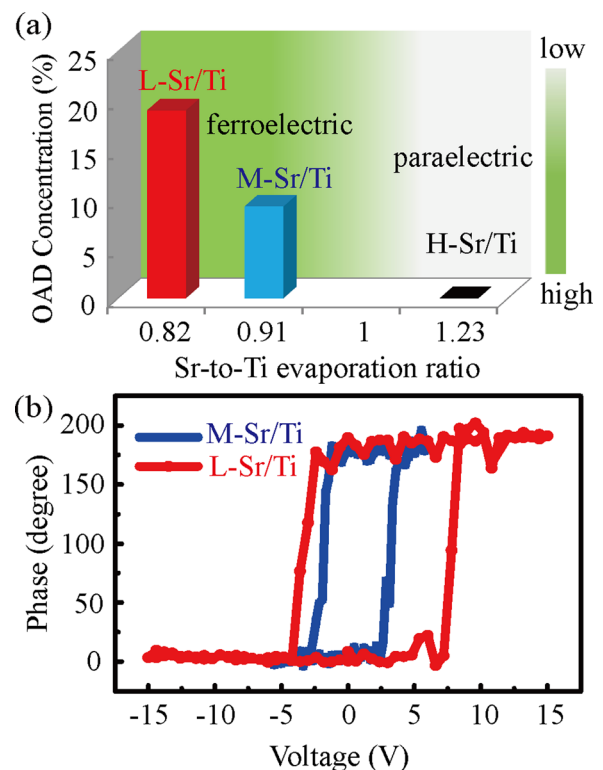


FIG. 3. (a) OADs concentrations of the L-Sr/Ti, M-Sr/Ti and H-Sr/Ti films. The background color indicates the coercive field, with the white zone on the right corresponding to the paraelectric region. (b) Phase hysteresis loops of L-Sr/Ti and M-Sr/Ti measured by the PFM at room temperature.

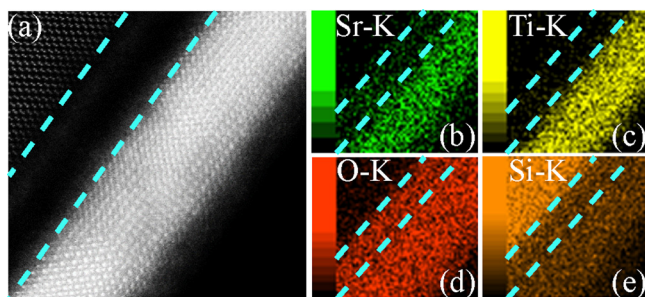


FIG. 4. (a) HAADF image of a nominal cation stoichiometric SrTiO<sub>3</sub> film grown on Si (001) substrate and (b)–(e) the corresponding EDX mapping of Sr-K, Ti-K, O-K, and Si-K signals, respectively.

concentration. Moreover, the high OADs concentration decreases the distances between them. As a consequence, the dipole-dipole interaction becomes stronger and further enhances the net polarization by aligning the  $+p$  dipole moments induced by individual OADs, and a high electric field is required to switch the polarization.<sup>15</sup> In brief, the more OADs in the film, the higher the coercive field it possesses. The upper limit of the OAD concentration can reach to 47% in the film with a Sr-to-Ti ratio of 0.68, while the crystallinity was not deteriorated by the large nonstoichiometry, i.e., sharp RHEED patterns and intensity oscillations were observed during growth. However, the large cation nonstoichiometry leads to the decrease in SrTiO<sub>3</sub> film resistivity,<sup>21</sup> which would lower the internal electric polarization. Considering such a compensation effect, the effective adjusting range of Sr-to-Ti ratio is  $\sim 0.8$  to  $\sim 1.2$ , which allows the reliable tuning of the FE coercive voltage up to 5.7 V.

It is noteworthy that even the nominal cation stoichiometric film may have OADs and thus show ferroelectric behaviors<sup>22</sup> because of the Sr diffusing towards the SrTiO<sub>3</sub>/Si interface. We employed the energy dispersive x-ray spectroscopy (EDX) mapping measurements with the STEM on the SrTiO<sub>3</sub> film grown with the Sr-to-Ti evaporation ratio of 1. Figure 4(a) is the HAADF image showing an amorphous layer forming at the SrTiO<sub>3</sub>/Si interface. All the Sr, O, and Si signals are detected in the amorphous layer, while Ti signal is only detectable in the crystalline film. The prominent Si-K signal in the film in Fig. 4(e) is an artificial effect due to the close energies of Si-K and Sr-L. The EDX results suggest that Sr tends to segregate at the heteroepitaxial interface, leaving a certain amount of Sr vacancies, consequently the induced OADs, in the SrTiO<sub>3</sub> film grown with the Sr-to-Ti evaporation ratio of 1 or even slightly higher. Correspondingly, the range of the cation concentration ratio for obtaining ferroelectricity is shifted towards the higher Sr/Ti ratio side, i.e., RTFE can be exhibited in the film with the Sr-to-Ti ratio slightly higher than 1, as labeled by the green region in Fig. 3(a).

In conclusion, high-quality single crystalline SrTiO<sub>3</sub> thin films with different cation concentrations have been prepared on Si (001) substrates by oxide MBE method. The RTFE in SrTiO<sub>3</sub> films is observed and ascribed to the existence of OADs associated by the cation nonstoichiometry. Furthermore, the coercive field of the ferroelectric SrTiO<sub>3</sub> films can be modulated by OADs concentration that is

controllable by means of tuning the metal evaporation rates during the MBE growth. This work opens a route towards engineering functional oxide electronic devices, such as oxide electronic devices controlled by multi-field through further combination of the ferroelectric SrTiO<sub>3</sub> templates and other functionalized materials such as ferromagnetic films.

This work was supported by Chinese MOST (Grant Nos. 2014CB921001 and 2012CB921702), NSFC (Grant Nos. 11404381 and 11225422), and the “Strategic Priority Research Program (B)” of the Chinese Academy of Sciences (Grant No. XDB07030100).

- <sup>1</sup>J. F. Scott, *Science* **315**, 954 (2007); H. Lu, X. Liu, J. D. Burton, C.-W. Bark, Y. Wang, Y. Zhang, D. J. Kim, A. Stamm, P. Lukashev, D. A. Felker, C. M. Folkman, P. Gao, M. S. Rzechowski, X. Q. Pan, C.-B. Eom, E. Y. Tsymlal, and A. Gruverman, *Adv. Mater.* **24**, 1209 (2012).
- <sup>2</sup>Q. Wang, Z. Li, W. Zhang, Z. Zhang, J. Zhang, W. Li, W. H. Ding, Y. Ou, P. Deng, K. Chang, J. Wen, C. Song, K. He, J. Jia, S. Ji, Y. Wang, L. Wang, X. Chen, X. Ma, and Q. Xue, *Chin. Rev. Lett.* **29**, 037402 (2012); X. Liu, D. Liu, W. Zhang, J. He, L. Zhao, S. He, D. Mou, F. Li, C. Tang, Z. Li, L. Wang, Y. Peng, Y. Liu, C. Chen, L. Yu, G. Liu, X. Dong, J. Zhang, C. Chen, Z. Xu, X. Chen, X. Ma, Q. Xue, and X. Zhou, *Nat. Commun.* **5**, 5047 (2014).
- <sup>3</sup>A. Ohtomo and H. Y. Hwang, *Nature* **427**, 423 (2004).
- <sup>4</sup>V. T. Tra, J.-W. Chen, P.-C. Huang, B.-C. Huang, Y. Cao, C.-H. Yeh, H.-J. Liu, E. A. Eliseev, A. N. Morozovska, J.-Y. Lin, Y.-C. Chen, M.-W. Chu, P.-W. Chiu, Y.-P. Chiu, L.-Q. Chen, C.-L. Wu, and Y.-H. Chu, *Adv. Mater.* **25**, 3357 (2013).
- <sup>5</sup>K. A. Müller and H. Burkard, *Phys. Rev. B* **19**, 3593 (1979); J. Hemberger, P. Lunkenheimer, R. Viana, R. Böhmer, and A. Loidl, *ibid.* **52**, 13159 (1995).
- <sup>6</sup>T. Mitsui and W. B. Westphal, *Phys. Rev.* **124**, 1354 (1961).
- <sup>7</sup>P. A. Fleury and J. M. Worlock, *Phys. Rev.* **174**, 613 (1968).
- <sup>8</sup>M. Itoh, R. Wang, Y. Inaguma, T. Yamaguchi, Y.-J. Shan, and T. Nakamura, *Phys. Rev. Lett.* **82**, 3540 (1999).
- <sup>9</sup>Y. S. Kim, D. J. Kim, T. H. Kim, T. W. Noh, J. S. Choi, B. H. Park, and J.-G. Yoon, *Appl. Phys. Lett.* **91**, 042908 (2007).
- <sup>10</sup>J. H. Haeni, P. Irvin, W. Chang, R. Uecker, P. Reiche, Y. L. Li, S. Choudhury, W. Tian, M. E. Hawley, B. Craigo, A. K. Tagantsev, X. Q. Pan, S. K. Streiffer, L. Q. Chen, S. W. Kirchoefer, J. Levy, and D. G. Schlom, *Nature* **430**, 758 (2004).
- <sup>11</sup>M. P. Warusawithana, J. A. Klug, H. Li, P. Ryan, L.-P. Wang, M. Bedzyk, D. A. Muller, L.-Q. Chen, J. Levy, and D. G. Schlom, *Science* **324**, 367 (2009).
- <sup>12</sup>H. W. Jang, A. Kumar, S. Denev, M. D. Biegalski, P. Maksymovych, C. W. Bark, C. T. Nelson, C. M. Folkman, S. H. Baek, N. Balke, C. M. Brooks, D. A. Tenne, D. G. Schlom, L. Q. Chen, X. Q. Pan, S. V. Kalinin, V. Gopalan, and C. B. Eom, *Phys. Rev. Lett.* **104**, 197601 (2010).
- <sup>13</sup>Y. S. Kim, J. Kim, S. J. Moon, W. S. Choi, Y. J. Chang, J.-G. Yoon, J. Yu, J.-S. Chung, and T. W. Noh, *Appl. Phys. Lett.* **94**, 202906 (2009).
- <sup>14</sup>D. A. Tenne, A. K. Farrar, C. M. Brooks, T. Heeg, J. Schubert, H. W. Jang, C. W. Bark, C. M. Folkman, C. B. Eom, and D. G. Schlom, *Appl. Phys. Lett.* **97**, 142901 (2010).
- <sup>15</sup>M. Choi, F. Oba, and I. Tanaka, *Phys. Rev. Lett.* **103**, 185502 (2009).
- <sup>16</sup>Z. Wang, F. Yang, Z. Zhang, Y. Tang, J. Feng, K. Wu, Q. Guo, and J. Guo, *Phys. Rev. B* **83**, 155453 (2011).
- <sup>17</sup>K. Hata, T. Kimura, S. Ozawa, and H. Shigekawa, *J. Vac. Sci. Technol., A* **18**, 1933 (2000).
- <sup>18</sup>A. Gruverman, O. Auciello, and H. Tokumoto, *Annu. Rev. Mater. Sci.* **28**, 101 (1998).
- <sup>19</sup>Y. Hamasaki, T. Shimizu, H. Taniguchi, T. Taniyama, S. Yasui, and M. Itoh, *Appl. Phys. Lett.* **104**, 082906 (2014).
- <sup>20</sup>E. Soergel, *J. Phys. D: Appl. Phys.* **44**, 464003 (2011).
- <sup>21</sup>F. Yang, Z. Yang, W. Li, F. Li, X. Zhu, L. Gu, H. D. Lee, S. Shubeita, C. Xu, T. Gustafsson, and J. Guo, *Sci. China-Phys. Mech. Astron.* **56**, 2404 (2013).
- <sup>22</sup>See supplementary material at <http://dx.doi.org/10.1063/1.4929610> for the PFM image of the film with Sr-to-Ti ratio of 1 during growth.